DYSPROSIA DOPED URANIUM DIOXIDE FUEL AND THE LAMBDA TRANSITION

M. Kleczek, B.J. Lewis[1], W.T. Thompson[2]
Royal Military College, Ontario, Canada

Abstract

Thermodynamic properties of solid and liquid UO_2, at temperatures above 2500 K, are rare and difficult to interpret. Low Void Reactivity Fuel (LVRF) employs Dysprosia in the originally natural Uranium fuel, but sufficient knowledge of solubility at all temperatures is still deficient. This paper describes research into the physical chemistry of UO_2-Dy_2O_3 mixtures, and includes an assessment of Dy_2O_3 effects on UO_2 at high temperatures. Specifically, research was conducted on the Lambda transition occurring at approximately 2670 K. The crystal structure determined by neutron diffraction and its effect on thermodynamic properties is discussed.

1. Introduction

The CANDU concept is currently being advanced with new fuel designs which offer greater performance and safety margins, and improved economics. To reduce the effects of a positive void coefficient in order to operate the four reactors at Bruce B at their design capacity, an innovative fuel design has been proposed which utilizes burnable neutron absorbers in the central element of CANFLEX fuel bundles. Though not yet in production, these enhanced modifications are now an intrinsic part of the fuel. The CANFLEX fuel bundle design was also adapted for early reactor models now operational and producing power. The central fuel element in each 43-element bundle can incorporate up to 10% by weight of Dy_2O_3 in otherwise natural UO_2. The other fuel elements contain slightly-enriched uranium. Compared to uranium, dysprosium has a very high neutron capture cross-section allowing it to be an ideal candidate for flux control. Overall, the CANFLEX fuel bundles enhance the efficiency of the existing CANDU reactor.

2. Lanthanides

In the lanthanide series, several members are fissionable products with the capability of dissolving in UO_2. In this developing technology, the LEU's outer fuel elements surround a central element containing a significant addition of dissolved dysprosia. In the advanced CANDU fuel bundle, certain lanthanide sesquioxides (Ln_2O_3) notably Dy_2O_3, have spawned a considerable amount of interest as a burnable neutron poison.

Several lanthanide sesquioxides are fission products soluble to a degree in UO_2 and capable of accumulating in the fuel of the CANDU during burn-up. They are a series of 15 rare-earth metallic elements with atomic-number designators 57-71; collectively formulated as Ln_2O_3. A rhombohedral phase (ULn_6O_{12}) may form when the mixture (or solution) of UO_2 and

---

[1] Thesis Supervisor

[2] Thesis Supervisor

Ln_2O_3-type oxides are exposed to oxidizing conditions. When heated in air or steam above 500°C, UO_2 oxidizes to a hyperstoichiometric oxide; commonly described as UO_{2+x}. High concentrations of Ln_2O_3, in CANDU doped fuel (Ln=Dy), have presented previously unknown issues associated with the sintering technology during the production of doped fuel pellets. This situation also bears concern over its behavior within the reactor should the fuel element develop a sheathing breach if contact is made with the heavy water (D_2O).

3. Crystal Structure of UO_2 and Dy_2O_3

Pure Dy_2O_3 exists in three crystal structures: cubic, monoclinic and hexagonal. A cubic modification exists at room-temperature to approximately 1807°C and retains a structure similarity to UO_2. The arrangements of the oxide and metal ion sites, in both UO_2 and cubic Dy_2O_3, bear comparison to CaF_2 or fluorite structure (Figure 1).

Upon investigation, oxygen anions (O^{2-}) appear in all anion sites of UO_2. For Dy_2O_3 (Figure 2) a quarter of the oxide ion sites are vacant resulting in a different space group classification for cubic Dy_2O_3 (Ia3) and UO_2 (Fm3m). Cubic Dy_2O_3 is stable from 0°C to approximately 1170°C and is isomorphous with bixbyite, $(Mn,Fe)_2O_3$. Recognizing structural similarities, the formula mass for Dy_2O_3 is occasionally written as $DyO_{1.5}$. This selection of molar mass simplifies the thermodynamic equations, describing the Gibbs energy of mixing associated, with a continuous cubic solid solution from pure UO_2 to pure $DyO_{1.5}$ despite the differences in classification of crystal structures for component oxides. Solid solutions have a near random mixing of U^{4+} and Dy^{3+} ions on the cation sites surrounded by a cubic cage of oxide ions — half of these cages have no cations — with a progressively increasing fraction of oxide ion vacancies as the Dy^{3+} concentration increases.

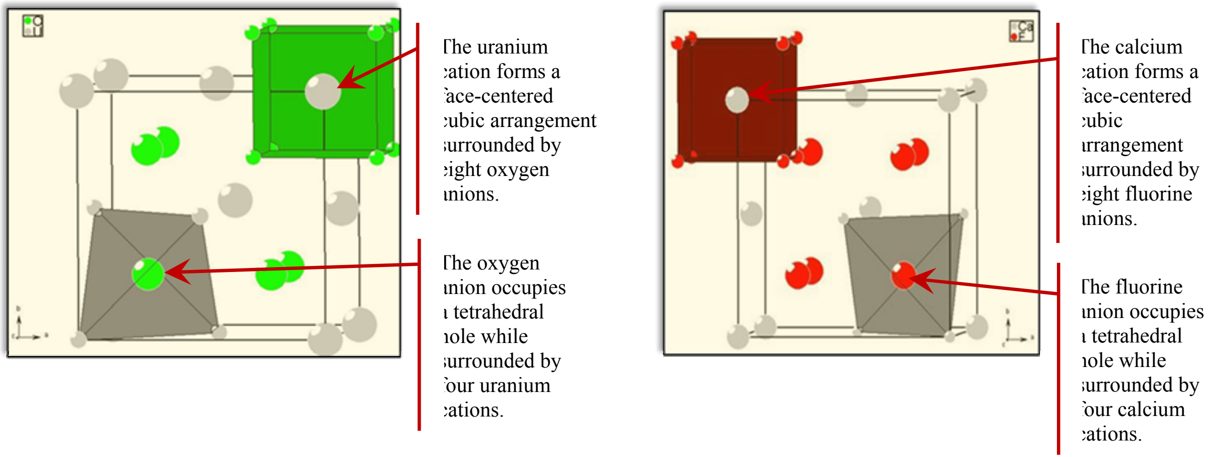

Figure 1a UO_2

Figure 1b CaF_2

Figure 1 Isomorphous unit cells of UO_2 and CaF_2.

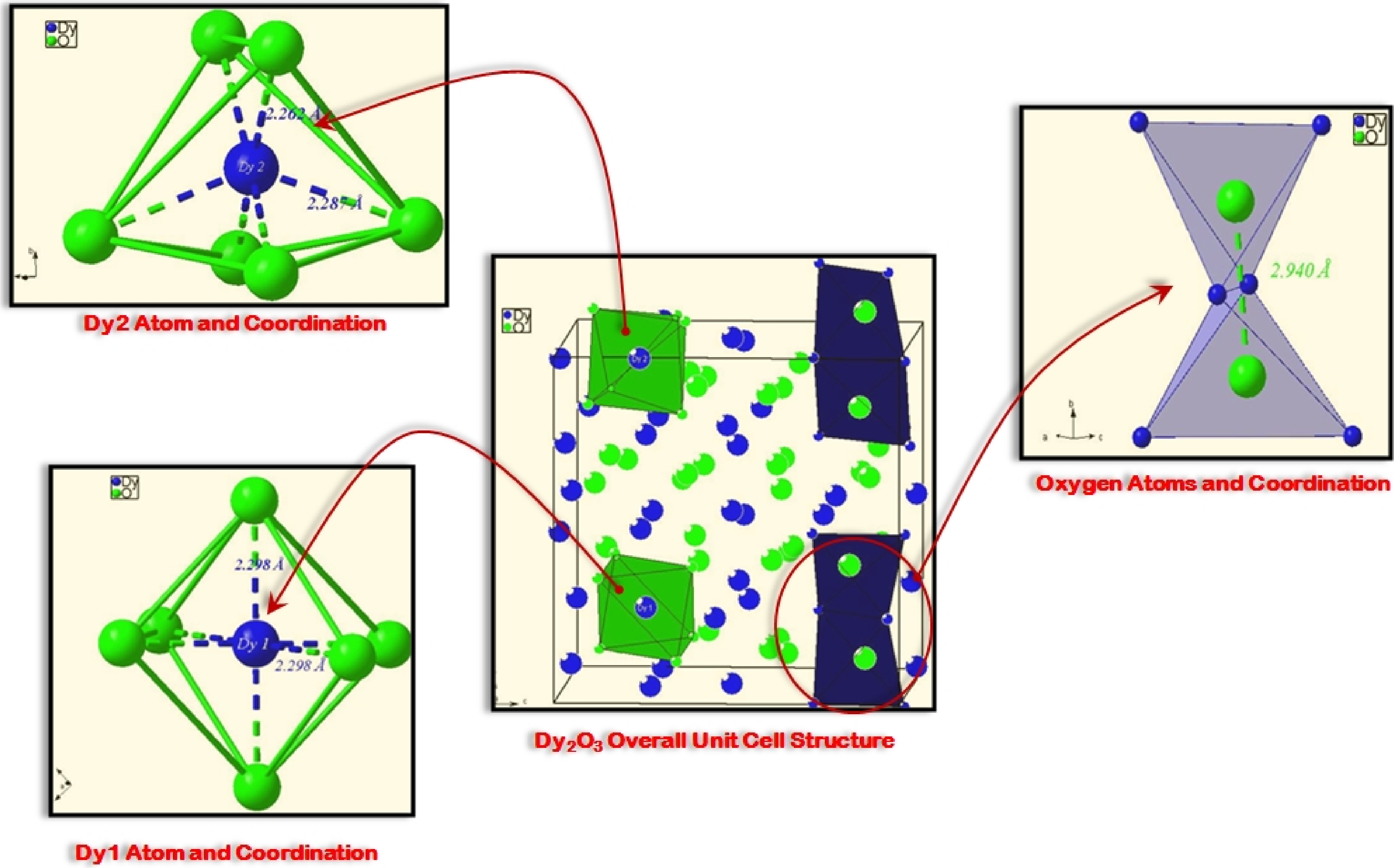

Dy2 Atom and Coordination

Oxygen Atoms and Coordination

Dy_2O_3 Overall Unit Cell Structure

Dy1 Atom and Coordination

Figure 2 Atom coordination about the Dy1, Dy2, and O in Dy_2O_3.

4. Coolant Void Reactivity

The current CANDU reactor has a positive void coefficient. This coefficient is defined as,

$$\alpha_V = \frac{d\rho}{dx} \tag{1}$$

where ρ is the reactivity and x the void fraction [1]. The definition of α_V demonstrates that an increase in the void fraction leads to an increase in reactivity. This is an undesirable situation from purely a safety point of view. However, the CANDU reactor has a large temperature coefficient, $\alpha_{T,}$ to compensate for this positive void coefficient. A typical scenario in safety failure commences with an increase in reactivity, power, excessive boiling, the creation of more voids, and back to an increase in reactivity. This cyclic process inevitably leads to significant amounts of liquid-coolant boiling and an undesirable power increase. Given this circumstance, it is desirable to have a negative void coefficient.

5. Lambda Transition of UO_2

The current work concerns the Lambda Transition of $UO_{2,}$ occurring at approximately 2670 K, and the effect that Dy_2O_3 additions may have on this matter. The speculation is that the transition temperature will decrease with an increase in concentration of dysprosia in the fuel.

Uranium dioxide, which crystallizes in the fluorite structure, has an oxygen sublattice thermally less stable than the uranium sublattice. The UO_2 experiences a phenomenon known as premelting. This is where at sufficiently high temperatures UO_2 becomes almost completely disordered with a large fraction of the oxygen anions occupying randomly regular or interstitial positions. The less stable oxygen sublattice displays higher in-solid mobility into the more stable uranium sublattice [2].

Many ionic biatomic crystals, with fluorite structures, exhibit an order-disorder transition into a superionic state at a temperature near 85% of the absolute melting temperature. This thermodynamic transition is confirmed by an increase in heat capacity as a function of temperature, with a characteristic lambda-shaped $C_p=C_p(T)$ curve. The occurrence of this transition is most likely due to the availability of large octahedral lattice voids; a characteristic of the fluorite structure. Neutron diffraction data confirms that the UO_2 forms a very high concentration of oxygen defects at high temperatures [3].

Heat capacity, $C_p(T)$, Figure 3, at high temperatures depends on a thermal energy exchange mechanism in the solid, and the presence of atomic and electronic defects. This pre-melting transition, or Lambda transition, is the result of the accessible creation of Frenkel defects in the mobile oxygen sublattice rendered cooperative by attractive interactions between complementary Frenkel defects (oxygen interstitials and vacancies). The quantitative degree of maximum disorder, realized just above the transition, is controlled by repulsive interactions between like defects [4]. In the same temperature range, electronic defects or localized small polarons provide only a minor contribution to C_p owing to electron hole interactions. Between 2700 K and T_m, the Schottky defects are expected to enhance the process. Above the melting point, the decrease in heat capacity is principally attributed to the saturation of the thermally activated contributions. The heat capacity, in liquid, is sustained by molecular vibrations up to 4500 K. Only at higher temperatures are more energetic electronic excitations thought to take place [5].

UO_2 can accommodate both oxygen interstitials and vacancies over a wide stoichiometry range ($1.5 \leq O/U \leq 2.25$) and at high temperatures. Thus, important variations of the melting point, with stoichiometry, result in conjunction with the appearance of an oxygen solubility gap with melting solid solutions of $UO_{2\pm x}$. Congruent melting of the stoichiometric dioxide is confirmed in Figure 3.

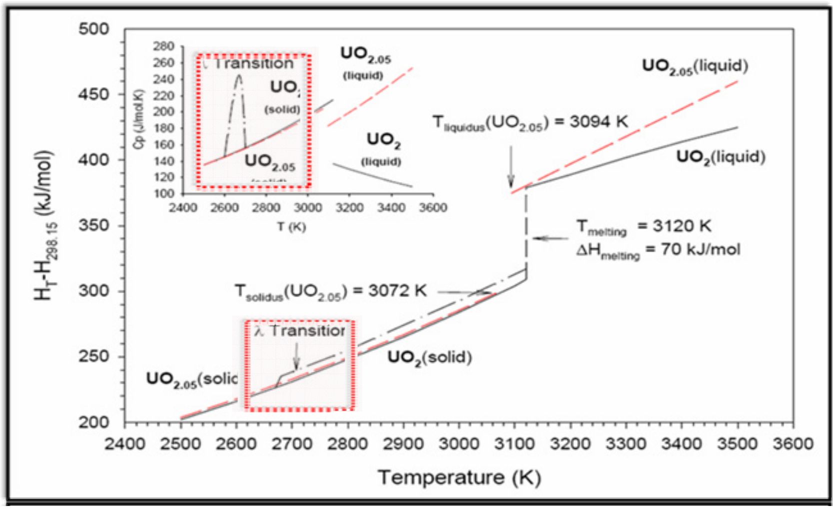

Figure 3 Two graphs depicting a Lambda transition for Temperature versus Enthalpy and Temperature versus Heat Capacity.

The heat capacity of nuclear oxide fuel is an important aspect of fuel physical chemistry involving rapid adiabatic core temperature excursions. Careful measurements of the thermodynamic properties for UO_2 above 2500 K are however rare and difficult to interpret [5].

6. Thermodynamics of the UO_2-Dy_2O_3 System

To compute the most stable system at various temperatures, pressures, and to establish different phases and species, a comparison of a range of Gibbs energies was required. This system gains stability as the Gibbs energy gains greater negativity; a determination based on its atomic distribution. This process, called Gibbs energy minimization, involves many systematic iterative computations.

The excess Gibbs energy is added to the ideal Gibbs energy of mixing based upon the random mixing of ions. The sum of the ideal, and the excess terms, provides the change in Gibbs energy when the components isothermally mix, or interdiffuse, forming a solid solution. A limitation on the extent of solid solubility exists, when the Gibbs energy of mixing is positive. The change in Gibbs energy must be negative or a solution will not form. In general, the ideal Gibbs energy of mixing for UO_2-$DyO_{1.5}$ systems is represented by this notation:

$$(1-X)UO_2 + XDyO_{1.5} = \{(1-X)UO_2 + XDyO_{1.5}\} \tag{2}$$

Pure cubic fluorite + pure cubic bixbyite = solid solution, where X is the mole fraction

$$\Delta G(\text{ideal}, UO_2\text{-}DyO_{1.5}) = X_{UO2}RT\ln[X_{UO2}] + X_{DyO1.5}RT\ln[X_{DyO1.5}] \tag{3}$$

where R is the gas constant , T is the temperature, and ΔG is the change in Gibbs Energy

In the UO_2-Dy_2O_3 system, the one phase solid solution involves the random placement of U^{4+} and Dy^{3+} within a fixed cubic oxide ion lattice. This translates to each mole of Dy_2O_3 providing 2-moles of Dy^{3+} cations. Alternatively, the molar mass of the lanthanide oxide might better be selected as $DyO_{1.5}$. The total number of mole components, based on the formula mass selected for one mole of UO_2-Dy_2O_3 mixture, is $1+X_{Dy2O3}$.

The mole fraction of $DyO_{1.5}$, when expressed using the system components UO_2 and Dy_2O_3, is noted as:

$$X_{DyO1.5} = 2X_{Dy2O3} / (1 + X_{Dy2O3}) \tag{4}$$

The notation for the ideal Gibbs energy of mixing for a mole of UO_2-Dy_2O_3 mixture is:

$$\Delta G^{ideal} = RT\{(X_{UO2})\ln[X_{UO2} / (1 + X_{Dy2O3})] + (2X_{Dy2O3})\ln[2X_{Dy2O3} / (1 + X_{Dy2O3})]\} \tag{5}$$

This expression recognizes the cation substituted solid solution without selecting UO_2 and $DyO_{1.5}$ as the system components.

The ideal Gibbs energy is minimized as a consequence of 2-ions per mole of Dy_2O_3, depicted in Figure 4, as compared to the 1-ion per mole system in Figure 5. This ideal mixing term provides a better baseline for describing the cubic UO_2-Dy_2O_3 solid solution. The Gibbs energy curves of the different phases are depicted in Figure 6.

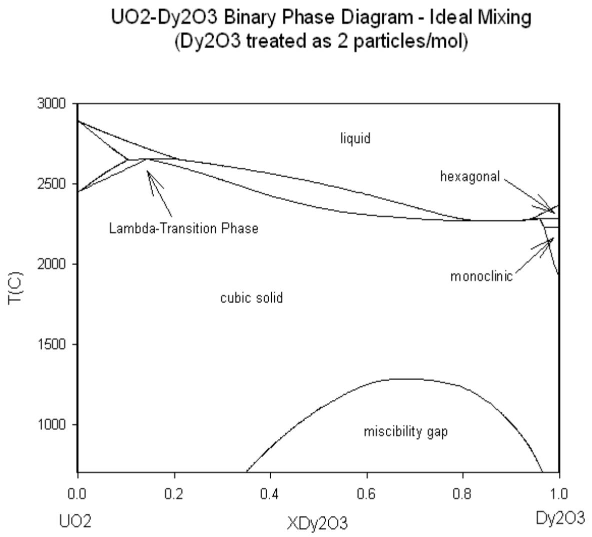

Figure 4 UO_2-Dy_2O_3 binary phase diagram with the lambda transition phase under ideal mixing conditions; Dy_2O_3 treated as 2 particles/mol.

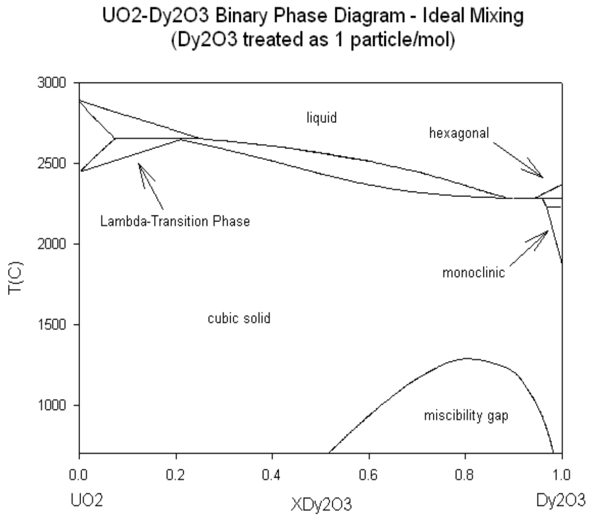

Figure 5 UO_2-Dy_2O_3 binary phase diagram with the lambda transition under ideal mixing conditions; Dy_2O_3 treated as 1 particle/mol, or $DyO_{1.5}$.

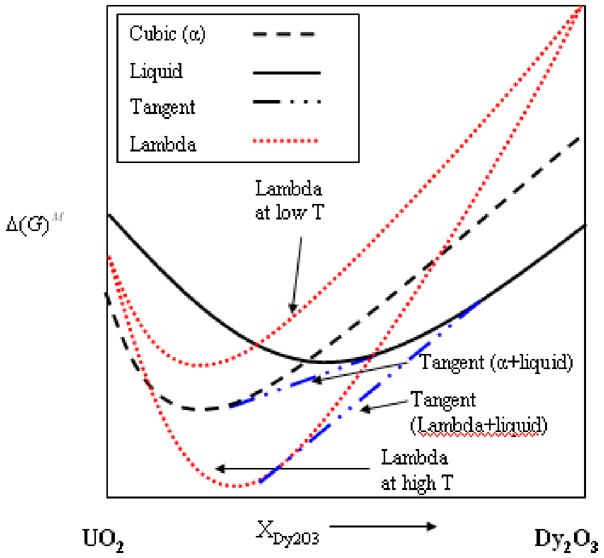

Figure 6 Gibbs energy curve of the UO_2-Dy_2O_3 system. The solid and liquid phases, along with the Lambda Phase at both lower and higher temperatures, are depicted.

The excess term chosen, in this UO_2-Dy_2O_3 system, was selected as:

$$G^E \ \alpha \ (X_{UO2})(X_{DyO1.5})^3 \tag{6}$$

As a result, in terms of UO_2 and Dy_2O_3, the previous equation now converts to:

$$G^E = p_0(X_{UO2})[2X_{Dy2O3} / (1 + X_{Dy2O3})] \tag{7}$$

In choosing p_0 as a single positive adjustable parameter, a method was devised to introduce immiscibility into the UO_2-Dy_2O_3 cubic solution. The power on $X_{DyO1.5}$ was chosen to skew the top of the miscibility gap to the Dy_2O_3 side of the system where the consolute condition is expected. The selected model for the mixing of the liquid phase was ideal and no excess term was added.

6.1 Non-Ideal Thermodynamic Conditions

A mixing term of +14 KJ/mol and -14 KJ/mol (Figures 7 and 8, respectively) for the UO_2-Dy_2O_3 system was investigated. The data revealed that the Lambda transition, for a system with a negative mixing term, first appeared at a lower temperature compared to the ideal mixing conditions; especially true when compared to a positive mixing term. For a negative Gibbs energy of mixing, the lambda phase expanded over a larger area, and range of the mole fraction of Dy_2O_3.

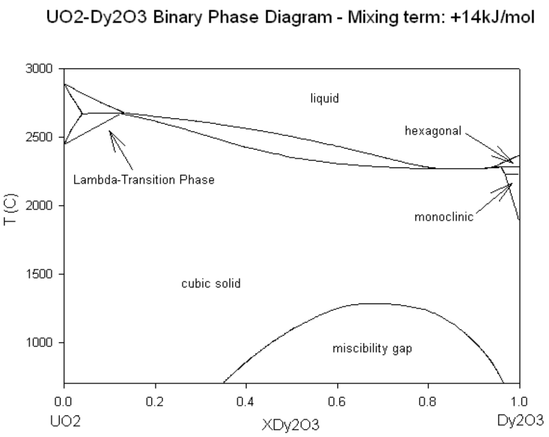

Figure 7 UO_2-Dy_2O_3 binary phase diagram with the lambda transition phase under a mixing condition of +14 kJ/mol.

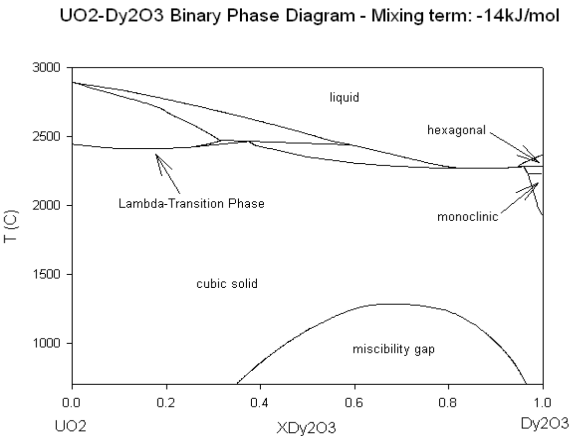

Figure 8 UO_2-Dy_2O_3 binary phase diagram with the lambda transition phase under a mixing condition of -14 kJ/mol.

A large difference in the phase diagrams is seen when comparing the UO_2-Dy_2O_3 under ideal mixing terms and a negative mixing term. The following figures show the change in the Lambda Phase region.

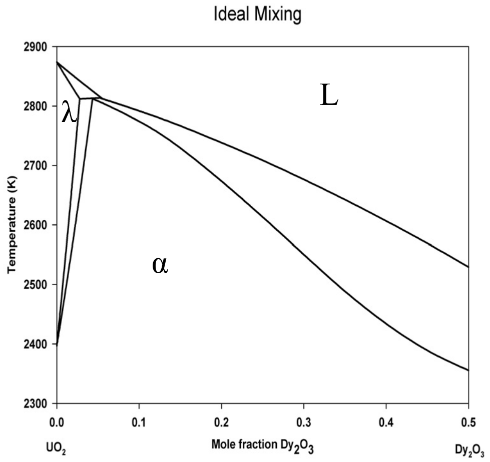

Figure 9 The Lambda Phase under ideal mixing.

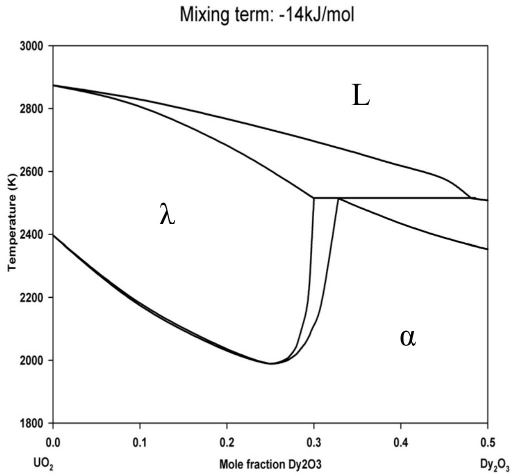

Figure 10 The Lambda Phase under negative mixing.

7. Crystal Structure Determination by X-Ray and Neutron Diffraction

High-temperature X-ray diffraction is used to study the thermal behavior of lattice constants, and detect and classify high temperature phases, and structural transitions. Neutron and X-ray diffraction patterns are characterized by peaks of specific heights, widths and positions. Rietveld refinement identifies crystalline materials using a least squares approach. Neutron diffraction measurements were conducted at Chalk River Laboratories on November 10 2008, employing UO_2 + 15% Dy to identify patterns at the minimum and maximum temperatures. No major change in crystal structure patterns, Figure 11, was seen between 308 K and 1803 K, except for a downshift of peaks and decrease in peak height at a higher temperature, which is to be expected. From this data, the thermal expansion coefficient can be determined and later applied towards fuel modeling and development. The Lambda Phase temperature of approximately 2670 K was not achieved. Further analysis will take place at the Los Alamos National Laboratory once their new furnace is built.

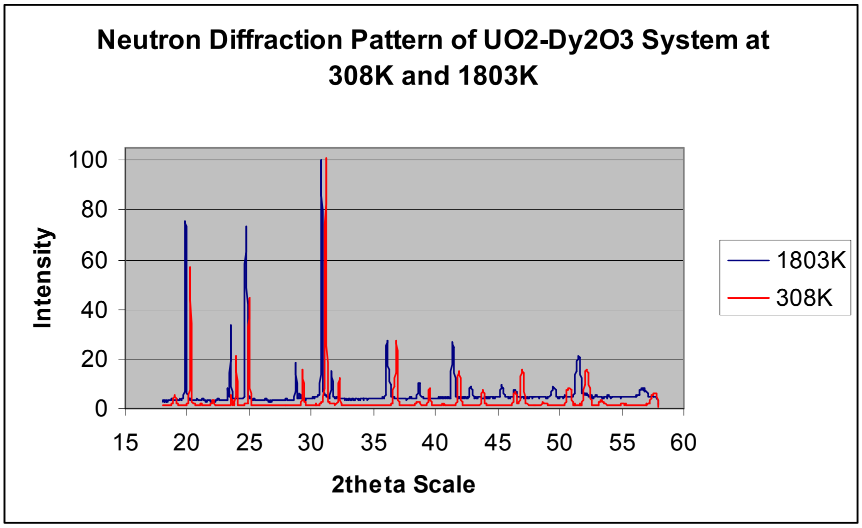

Figure 11 Neutron diffraction pattern of UO_2 + 15% Dy at 308 K and 1803 K.

8. Conclusion

Doped fuel (UO_2-Dy_2O_3) is currently being introduced to enhance the performance and safety of four units at Bruce B. As such, research is being conducted on the physical chemistry of UO_2-Dy_2O_3 mixtures at high temperatures, specifically the Lambda transition at approximately 2670 K. Crystal structure determination by neutron diffraction and thermal expansion coefficients are being determined in order to apply this knowledge to advance fuel modeling capabilities and development.

9. Acknowledgements

Gratitude goes forward to the staff at Chalk River Laboratories (CRL) for their work on obtaining the neutron diffraction patterns of our samples of UO_2 doped with dysprosia.

10. References

[1] J.R. Lamarsh and A.J. Baratta, "Introduction to Nuclear Engineering – Third Edition", Prentice Hall, New Jersey, 2001.

[2] J.K. Fink, "Thermophysical Properties of Uranium Dioxide", Journal of Nuclear Materials Vol. 279, 2000, pp. 1-18.

[3] C. Ronchi and G.J. Hyland, "Analysis of Recent Measurements of the Heat Capacity of Uranium Dioxide", Journal of Alloys and Compounds, Vol. 213/214, 1994, pp. 159-168.

[4] D. Manara, et al., "On the Present State of Investigation of Thermodynamic Properties of Solid and Liquid UO_{2+x}", Journal of Nuclear Materials, Vol. 362, 2007, pp. 14-18.

[5] Yakub, et al, "Molecular Dynamics Simulation of Premelting and Melting Phase Transitions in Stoichiometric Uranium Dioxide", The Journal of Chemical Physics, Vol. 127, 094508, 2007.